Talukder Z. Jubery[1]
Anmiv S. Prabhu[2]
Min J. Kim[2]
Prashanta Dutta[1]

[1]School of Mechanical and Materials Engineering, Washington State University, Pullman, Washington, USA
[2]School of Biomedical Engineering, Science and Health Systems, Drexel University, Philadelphia, PA, USA

Received March 31, 2011
Revised July 11, 2011
Accepted July 20, 2011

Research Article

Modeling and simulation of nanoparticle separation through a solid-state nanopore

Recent experimental studies show that electrokinetic phenomena such as electroosmosis and electrophoresis can be used to separate nanoparticles on the basis of their size and charge using nanopore-based devices. However, the efficient separation through a nanopore depends on a number of factors such as externally applied voltage, size and charge density of particle, size and charge density of membrane pore, and the concentration of bulk electrolyte. To design an efficient nanopore-based separation platform, a continuum-based mathematical model is used for fluid. The model is based on Poisson–Nernst–Planck equations along with Navier–Stokes equations for fluid flow and on the Langevin equation for particle translocation. Our numerical study reveals that membrane pore surface charge density is a vital parameter in the separation through a nanopore. In this study, we have simulated high-density lipoprotein (HDL) and low-density lipoprotein (LDL) as the sample nanoparticles to demonstrate the capability of such a platform. Numerical results suggest that efficient separation of HDL from LDL in a 0.2 M KCL solution (resembling blood buffer) through a 150 nm pore is possible if the pore surface charge density is $\sim -4.0\,\mathrm{mC/m^2}$. Moreover, we observe that pore length and diameter are relatively less important in the nanoparticle separation process considered here.

Keywords:
Electrokinetic / Nanoparticles / Nanopore / Separation
DOI 10.1002/elps.201100201

1 Introduction

Rapid separation of naturally occuring nanoparticles such as renal calculus, lipoproteins, and virions is necessary for various biomedical applications [1–3]. Existing separation techniques utilize an immobilized matrix such as a polymeric gel or a chromatographic column to separate individual fractions from a mixture. These matrices contain randomly oriented pores with wide size distributions, which cannot be easily measured, controlled, and manipulated. This lack of engineering control is a major drawback of such techniques and greatly affects their efficiency [4]. Recently, nanoscale architectures of various geometries are being investigated for the development of next-generation separation and detection devices [5, 6] because within these devices the transport properties of nanoparticles can be closely controlled, and thus making them ideally suited for efficient nanoparticle separation. Among these devices solid-state nanopores fabricated in ultra-thin substrates are prominent.

Solid-state nanopores are generally fabricated on silicon dioxide (SiO_2) or silicon nitride (Si_3N_4) membranes using a focused ion beam [7], electron beam [8], or various asymmetric etching techniques [9]. Moreover, the surface properties such as hydrophobicity [10, 11] and surface charge density [12, 13] of the nanopore membrane can be modified to precisely control the transport of particles across the nanopore. In a seminal work, Striemer et al. [14] reported that a chemcially modified nanoporous membrane can be used to separate two common blood proteins (bovine serum albumin and immunoglobulin-γ) based on their size and charge density. Their membranes were $\sim$10 nm thick and pore sizes ranging from 5 to 25 nm. Similarly, Savariar et al. [11] demonstrated the separation of *p*-nitrotoluene and *p*-nitrophenol based on their hydrophobicity using a nanopore device. In both these studies, separation was based on the passive transport across an optimized nanoscale architecture. However, active driving mechanisms such as pressure-driven flow or electric field-driven transport can also be used to get faster and high-throughput separation in a directed and controlled manner. Moreover, active transport

Correspondence: Dr. Prashanta Dutta, School of Mechanical and Materials Engineering, Washington State University, Pullman, Washington 99164, USA
E-mail: prashanta@wsu.edu
Fax: +1-509-335-4662

Abbreviations: EDL, electric double layer; **HDL,** high-density lipoprotein; **LDL,** low-density lipoprotein; **MD,** molecular dynamics

Colour Online: See the article online to view Figs. 1–7 in colour.

of biological nanoparticles across a nanopore can be used to reveal the type and composition of proteins [15].

In an active transport setup, a nanopore-bearing membrane is generally placed between two reservoirs (cis and trans), and an external voltage difference (electrokinetic transport) or a pressure gradient or a combination of both is applied across the membrane to drive the nanoparticles through the pore. Firnkes et al. [16] showed that electrokinetic transport of model proteins (avidin) through a silicon nitride (Si_3N_4) nanopore can be controlled by modifying the ζ potential or surface charge density of pore. More recently, Prabhu et al. [17] presented an electrokinetic-based nanopore device to control the permeability rate of different types of polysterene beads by chemically modifying the membrane surface.

To design an effective nanofluidic platform for particle separation, it is necessary to analyze the physics of particle translocation through such a device since the translocation process is affected by various parameters, such as externally applied voltage, size and charge density of particle, size and charge density of membrane, and the concentration of the bulk electrolyte. Theoretical modeling of this translocation through nanopore has been studied extensively by molecular dynamics (MD) techniques [18]. However, MD is generally suitable for a relatively smaller computational domain with spatial dimensions on the order of 100 nm as well as very short time scale (less than a microsecond), and hence MD cannot be used for device-level simulation [19]. To circumvent the limitations of the very short time and length scales of molecular simulation, several research groups have used continuum-based models for electrokinetic transport of charged cylinderical [20] and spherical particles [21] through a nanopore. But those models considered (A) only a single particle and (B) a much shorter calculation domain than an actual nanofluidic device. Therefore, to study the separation of particles through an electrokinetic-based nanopore device it is necessary to develop a numerical model which can take care of multi-particle translocations in an actual physical domain.

In this work, we have used a mathematical model based on mass, charge, and momentum conservation equations to study multiple particle translocations through a nanopore. This general model can deal with all parameters affecting particle translocation. The objective of this work is to systematically study the effect of different operating parameters for the separation of two different types of particles: Particle A (10 nm diameter and $-7.0\,\mathrm{mC/m^2}$ surface charge) and Particle B (30 nm diameter and $-3.3\,\mathrm{mC/m^2}$ surface charge) using a multi-domain numerical method. Particles A and B closely resemble high-density lipoprotein (HDL) and low-density lipoprotein (LDL), respectively.

2 Mathematical model and numerical method

In the actual experiments, the nanoparticles are generally suspended in an electrolyte solution. The electrolyte influences particle translocation and hence our approach is to study the surrounding electrolyte in order to understand the physics of particle translocation. Based on the continuum approximation, the mass and momentum conservation equations for this electrolyte solution can be expressed as Nernst–Planck and Navier–Stokes equations, respectively.

The net transport of ionic species of an electrolyte is described by the Nernst–Planck equation:

$$\frac{\partial C_i}{\partial t} + \nabla \cdot (-D_i \nabla C_i + \vec{V} C_i + z_i \omega_i \vec{E} C_i) = R_i \tag{1}$$

where D_i, ω_i, R_i, z_i, and C_i are the molecular diffusivity, mobility, rate of production, valence, and concentration of the ith ionic species, respectively. $\vec{V}$ is the velocity of bulk electrolyte and $\vec{E} = -\nabla\varphi$, is the electric field. The electric potential (φ) distribution in the electrolyte is based on Gauss's electrostatic theorem

$$\nabla \cdot (\varepsilon \nabla \varphi) = -\rho_e \tag{2}$$

where ε is the permittivity of the electrolyte, ρ_e is the electric charge density, which is given by $\rho_e = \sum_{i=1}^{N} F z_i C_i$, where F is the Faraday constant. Equation (2) is also known as the Poisson equation. The flow of an incompressible electrolyte is governed by the Navier–Stokes equation [22]

$$\rho_f \left(\frac{\partial \vec{V}}{\partial t} + (\vec{V} \cdot \nabla \vec{V}) \right) = -\nabla P + \mu \nabla^2 \vec{V} + \rho_e \vec{E} \tag{3}$$

where ρ_f, P, and μ are the electrolyte density, pressure, and viscosity, respectively. Moreover, the incompressibility condition requires a divergence-free velocity field given by

$$\nabla \cdot \vec{V} = 0 \tag{4}$$

Particle motion within electrolyte suspension is governed by the Langevin equation

$$m_{pi} \frac{d\vec{V}_{pi}}{dt} = \vec{F}_{Di} + \vec{F}_{Ei} + \vec{F}_{Bi} \tag{5}$$

where m_{pi} and $\vec{V}_{pi}$ are mass and velocity of ith particle. $\vec{F}_{Di}$, $\vec{F}_{Ei}$ and $\vec{F}_{Bi}$ are hydrodynamic drag force, electrokinetic force, and Brownian motion force respectively. Of these, the hydrodynamic force $\vec{F}_{Di}$ acting on a particle can be calculated from [23] as

$$\vec{F}_{Di} = \int\int_S \left[-P\vec{\vec{I}} + \mu((\nabla \vec{V} + \nabla \vec{V})^T) \right] \cdot \hat{n} dS \tag{6}$$

where $\vec{\vec{I}}$ is the identity tensor and $\hat{n}$ is the unit normal. The electrokinetic force $\vec{F}_{Ei}$ depends on the electric field around the particle surface (S) as [23]

$$\vec{F}_{Ei} = \int\int_S \varepsilon \left[\vec{E}\vec{E} - \frac{1}{2}\left(\vec{E} \cdot \vec{E}\right)\vec{\vec{I}} \right] \cdot \hat{n} dS \tag{7}$$

And the Brownian motion force can be found form the following model equation [24]:

$$\vec{F}_{Bi} = m_{pi} \vec{B} \tag{8a}$$

$$B_j = G_j \sqrt{\frac{216 \mu k_B T}{\nabla t \pi \rho_f d^5 r^2 C_c}} \tag{8b}$$

where B_j are components of $\vec{B}$, T is the absolute temperature, k_B is the Boltzmann constant, d is the diameter of the particle, Δt is the time step used for numerical time integration, r is the ratio of the density of particle to the density of fluid, G_j is a Gaussian random variable with zero mean and unit variance, and C_c is the Cunningham slip correction factor.

2.1 Assumptions

In the electrolyte system, the ionic association–dissociation process is very fast. Thus, in the Nernst–Planck equation, the source term due to chemical reaction is neglected. Moreover, we have neglected electrochemical reactions at both anode and cathode. We have also neglected the unsteady term from the Nernst–Planck equation as the characteristic time scale for local ionic species concentration change is $(d^2/D) \approx O(10^{-9})$ s in the nanopore-based platform. This small characteristic time suggests that local concentration distribution can be considered at equilibrium at every instant. The model also neglects the unsteady term of Navier–Stokes equation because the characteristic time scale $(\rho_f d^2/\mu)$ for local velocity change is very small, $O(10^{-10})$ s. The advection term in Navier–Stokes equation is also dropped due to the low Reynolds number ($Re \ll 1$) creeping flow of the electrolyte through the nanoscale device. In this study, particle motion is considered to be quasi-steady since inertia of the system (surrounding electrolyte) is negligible [25], and hence the unsteady term in the Langevin equation is also neglected. Unlike microparticle translocation, the contribution of the angular velocity is not considered here because of its negligible contribution to the particle translocation velocity.

2.2 Computational domain and boundary conditions

Figure 1A shows the schematic of the nanofluidic platform used for the separation of particles. In this case, the nanopore is at the center of the membrane which is placed between two cylindrical microfluidic reservoirs. Since the device modeled here involves length scales ranging from nanometers (Debye length) to microns (membrane width) to millimeters (dimensions of reservoir), a multiscale model is developed to predict the fluid flow and particle translocation behavior. A very fine domain close to the pore (Fig. 1B) is selected to accurately model the electrokinetic forces acting on fluid and particles, while the entire domain (Fig. 1A) is simulated to obtain the boundary conditions for the finer (dashed) region.

For the regular domain (Fig. 1A), in solving Poisson's equation for electrostatic potential, specified surface charge density was set for membrane surfaces and a specified potential was assigned at the top and bottom boundaries. In solving the Navier–Stokes equation, normal flow with $P = 0$ was used as the boundary condition for top and bottom surfaces. A no-slip velocity condition was assumed on all other solid boundaries. For the Nernst–Plank equations, specified concentration was used at the top and bottom boundaries and zero (normal) flux was considered at all other boundaries. On the other hand, for the finer domain (Fig. 1B) boundary conditions were obtained from the solution of the electric field, concentration distribution, and flow field in the regular domain without the presence of any particles. In the fine domain calculations the presence of particles was taken into consideration, and the boundary conditions used on the particles' surface were; no slip for Navier–Stokes equation, specified surface charge for Poisson's equation, and zero (normal) electromigration and diffusion flux for Nernst–Planck equations. Table S1 shows the expressions used for boundary conditions on particle and pore surfaces.

2.3 Numerical model

In this study, we seek to separate nanoparticles effectively by applying an external electric field in the system. Under the

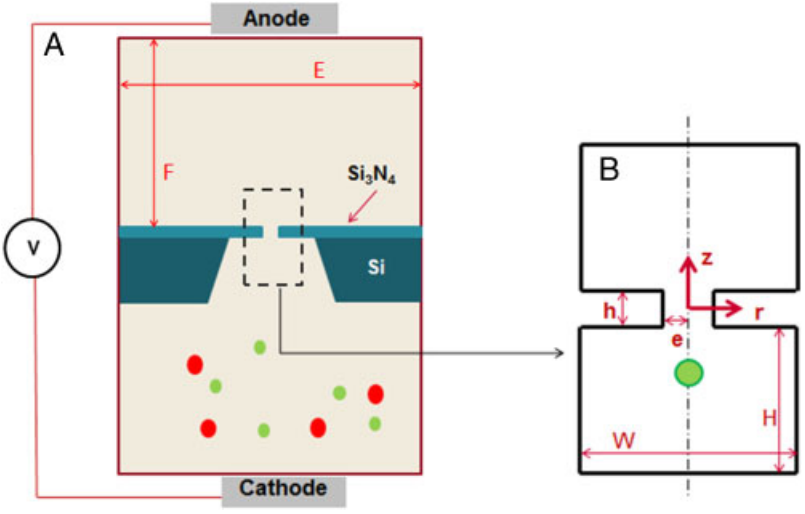

Figure 1. Schematic of the computational domain used in this study for (A) regular and (B) finer domain. The regular computational domain consists of two cylindrical compartments of diameter (E) and height (F) and separated by an insulating membrane with a pore at the center. The system is considered to be filled with an electrolyte and a voltage bias is considered across the pore. The length scale of the regular domain is the same as a physical device. The fine domain is enclosed by the dashed lines in the regular domain (not to scale). The fine domain consists of two cylindrical compartments of diameter (W) and height (H) separated by an insulating membrane of height (h) with a pore of radius (e). The insulating membrane was assigned a surface charge density (σ_m). In the fine domain, spherical particles were introduced along the centerline of pore.

action of the electric field, the various forces acting on the particles are the Brownian motion force, the electrokinetic force, and the hydrodynamic drag force. The Brownian effect can be avoided by using a variable time step in the particle velocity calculation process. For instance, close to the pore the Brownian motion force (Eq. 8) is small compared with the electrokinetic force (Eq. 7), and a small time step can be used to predict the particle location without considering the Brownian force. On the other hand, further away from the pore considering large time steps nullifies the net Brownian effect.

For calculating particle's location, we used a quasi-steady method [25] which assumes that fluids and particles are in equilibrium at any instant. Based on this quasi-steady assumption, the equation of motion for the particles can be expressed as follows:

$$\vec{F}_{\mathrm{Di}}+\vec{F}_{\mathrm{Ei}}=0 \tag{9}$$

and the particle velocity can be found by satisfying Eq. (9). Finally, the ionic current through the nanopore is calculated as follows:

$$I_{\mathrm{C}}=\int\int_{A}\sum_{\mathrm{i}=1}^{\mathrm{N}} Fz_i\left(-D_i\nabla C_i+\vec{V}C_i+z_i\omega_i\vec{E}C_i\right)\cdot \mathrm{d}\vec{A} \tag{10}$$

where A is the cross-sectional area of the nanopore and N is the number of ionic components in the electrolyte.

3 Numerical scheme

A 2D axisymmetric finite element-based method was used for this study. The finite element calculations were performed using quadratic triangular elements. Since the accuracy of the numerical solutions strongly depends on the mesh size, a refined mesh is necessary in the region near the surface where the gradients of the dependent variables are pronounced. In this study, a finer mesh was used near the charged membrane surface in order to capture the subtle changes in the potential, ionic concentration, and velocity. However, a less dense mesh was used in the regular domain for computational speed.

In order to solve the coupled governing equations, an initial value for particle velocity was assumed and Eqs. (1–4) were solved simultaneously with an iterative scheme. For the convergence criteria, absolute relative error between two successive iterations was set $<10^{-6}$ for each dependent variable. Since we used a set of guess values for velocity of particles, they would not satisfy the quasi-steady condition (Eq. 9). Therefore, the particle velocities were updated iteratively using the Newton–Raphson method until the electrostatic force acting on each particle was balanced by the hydrodynamic drag. The hydrodynamic and electrostatic forces are calculated from Eqs. (6) and (7). Finally, particle positions were updated explicitly using variable time steps. Time steps considered were 10^{-5} s when the particle is far away from the pore and 10^{-6} s when the particle is close to the pore.

4 Model validation

In order to verify this model, nanoparticle translocation across a nanofluidic platform was carried out. The experimental setup consisted of two electrolytic half-cells formed by identical microfluidic chambers of height, $F = 5$ mm and diameter, $E = 1$ mm. A single 150 nm pore was fabricated in a 50-nm-thick free standing, low-stress silicon nitride membrane by focused ion beam milling and housed in between the chambers. Prior to placing in the chamber, the membrane was chemically modified with (3-aminopropyl) triethoxysilane to change its surface charge density. A mixture of sulfate functionalized polystyrene beads with a mean diameter of 22 nm (with a range from 10 to 30 nm) and surface charge density of -22 mC/m^2 were diluted in 0.2 M KCl and 1% Triton X-100 buffer to a final concentration of 10^5 particles per milliliter. A 350 mV voltage bias was applied across the chamber and the current across the pore was measured using a patch clamp amplifier (AXOPATCH 200B, Molecular Devices). A transient drop in current was observed each time a bead translocated through the pore due to the temporary displacement of the electrolyte within the pore by the bead.

For numerical simulation of (full) device domain, the experimental ionic (bulk) concentration and bias potential were used to obtain the flow and electric fields. On the other hand, for the finer computational domain the height (H) and radius (B) were set as 600 nm, and a single 30 nm diameter particle with a surface charge density of -22 mC/m^2 was allowed to translocate through the nanopore. The magnitudes of H and B are chosen large enough so that further increases in H or B has little effect on the computational results, but small enough to simulate the problem with available computer memory. The pore surface charge density was set to -15 mC/m^2, which approximates the surface charge density of the chemically modified pore used in the experiment. All other boundary conditions are obtained from the simulation of the full domain. Figure 2 depicts the computed and experimental ionic current drop as a function of particle position. Our numerical results are in good agreement with the experimental observations for a 30 nm bead translocating through a 150 nm pore.

5 Results and discussion

The primary objective of this work was to design an optimum electrokinetic-based nanofluidic platform for the separation of one type of nanoparticle from another. To demonstrate the capability of the numerical tool, we selected LDL apheresis as our model system. In LDL apheresis, a medical procedure, LDLs are separated from other lipoproteins (mainly HDLs) in the blood plasma. To model this process, we have selected two types of particles (particles A and B) which imitate HDL and LDL, and 0.2 M KCl was set as the electrolyte to mimic blood serum. At this concentration, the thickness of the electric double layer (EDL) close to

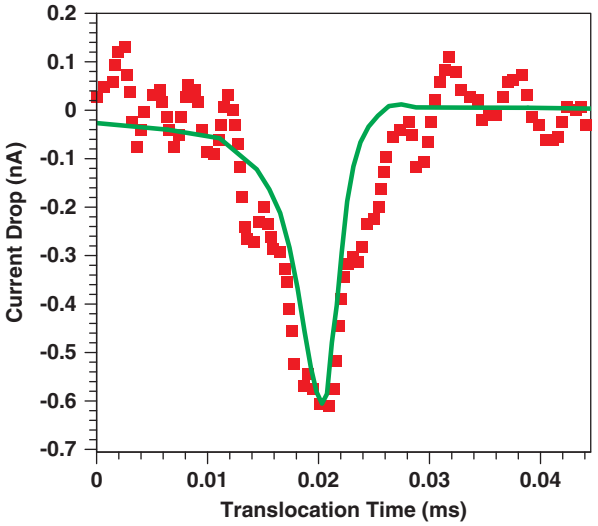

Figure 2. Ionic current drop generated in the system by a 30 nm spherical particle with a surface charge density $-22\ mC/m^2$ passing through the nanopore. Here $\sigma_m = -15\ mC/m^2$, $E = 1$ mm, $F = 5$ mm, $H = 600$ nm, $W = 1200$ nm, $h = 50$ nm, $e = 75$ nm and $C_o = 0.2$ M. The solid line and symbols correspond to numerical simulation and experimental results, respectively.

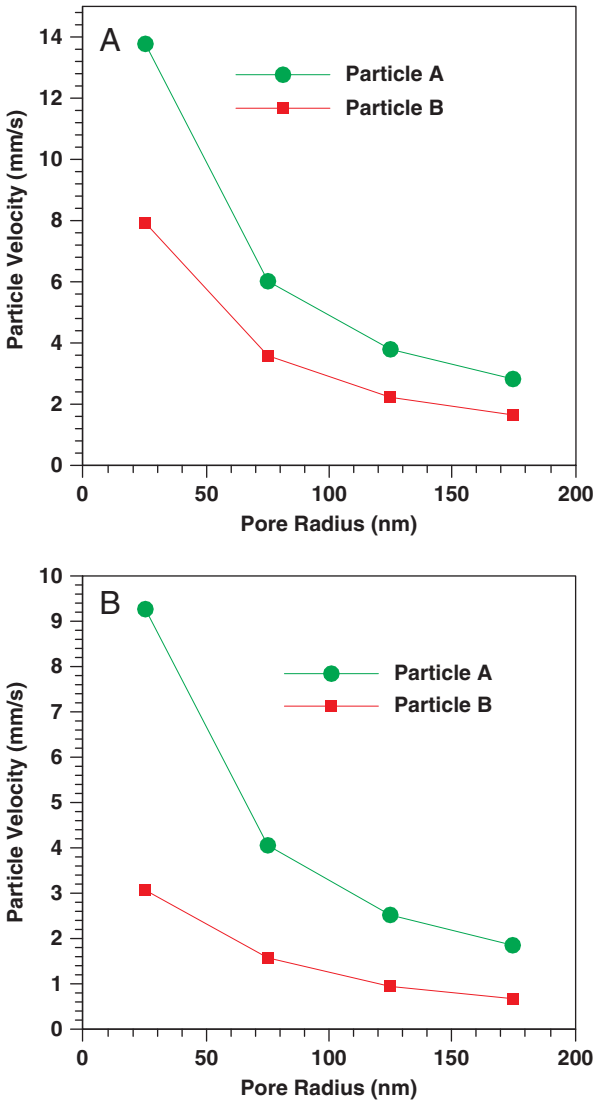

Figure 3. Particle velocity (A) across an uncharged membrane ($\sigma_m = 0.0\ mC/m^2$) and (B) across a membrane with surface charge density $\sigma_m = -2.0\ mC/m^2$ as a function of pore radius. Particle A: 10 nm diameter and $-7.0\ mC/m^2$ surface charge and Particle B: 30 nm diameter and $-3.3\ mC/m^2$ surface charge. All other simulation conditions are the same as in Fig. 2.

the charged surfaces is ≈ 0.7 nm which eliminates the possibility of any EDL overlap between them. Hence, the charge regulation of pore and particles could be neglected in the model and the surface charge density was considered constant.

In our electrokinetic-based nanofluidic platform (Fig. 1), the translocation of the nanoparticle through a pore depends on a number of parameters, such as the applied voltage bias, pore diameter, pore thickness, and membrane surface properties. It is well established that the applied voltage bias has only a linear effect on particle translocation and it cannot be used as a key parameter for device design. Thus, we have considered other parameters to study the translocation of particles A and B through a nanopore in a 0.2 M KCl solution using a nominal external potential of 350 mV. For the rest of the discussion, the overall size of the computation domain is the same as Section 4, but the pore size and pore surface properties are varied from case to case.

5.1 Effect of pore size

At first, we considered only one particle in the system, either particle A or particle B on the axis of the pore ($r = 0$ and $z = 0$). In this configuration, a positive particle velocity (toward anode) suggests that particle will translocate through the pore. If one type of particle experiences a positive velocity, while the other a negative velocity then, it is possible to achieve separation through the nanopore. Since both types of particles are negatively charged, they will tend to move toward the anode under the action of the electric field albeit at different speeds. However, if the nanopore membrane is also charged, then the translocation phenomena will not be straight forward due to the complex interaction among particles, surrounding fluid, and the membrane.

Figure 3 indicates a positive velocity for particle A at the center of the pore with an uncharged as well as a slightly negatively charged pore surface. However, as the pore radius increases, particle velocity decreases and asymptotically approaching zero at much higher pore radius. This is because of a reduction in the electric field strength around the particle in case of larger pores which eventually reduces the electrokinetic force acting on the particle. The same phenomenon is also found in case of Particle B. As both particles continue to experience a positive velocity, the pore

radius is not a useful control parameter for particle separation. Our study also reveals that pore thickness has a similar effect on particle translocation, where the particle velocities remain positive (upward) for both types of particles.

5.2 Effect of membrane pore charge

Next, we study the effect of membrane surface charge density on particle translocation by varying its value from $-20\,mC/m^2$, which is the typical of Si_3N_4 to $20\,mC/m^2$. As in the previous section, only one type of particle is placed in the computational domain at a time to investigate the effect of pore charge. Figure 4A shows the particles' velocity at the center of the pore for five different membrane charges. For a highly positive surface charge density ($20\,mC/m^2$), both particles have a positive velocity. However, as the pore surface charge decreases the particle velocity decreases, eventually becoming negative for a highly negatively charged membrane. This is because of the combined effect of electrophoresis and electroosmosis in the system. Under the action of external electric field, negatively charged particles will experience an electrophoretic force (EF) toward the anode (positive z direction), but the electroosmotic contribution due to the particle charge will be toward the cathode (for negative pore charge) which produces a retardation effect and tends to reduce the particle electrophoretic velocity. The electroosmotic contribution due to membrane charge depends on the nature and magnitude of membrane surface charge. For instance, if the pore surface charge density is positive, the direction of the electroosmotic flow is toward the anode and vice versa. Thus, by controlling the membrane surface charge density, the particle's net velocity can be increased, decreased, or even reversed.

Figure 4 also reveals that the overall particle velocity trend is the same for both particles, but the translocation rate is slower for Particle B due to the lower particle charge density and larger size. Therefore, to separate the two types of particles in the electrolytes one has to select appropriate magnitude and type of pore surface charge density. Our hypothesis is that by drawing a best-fit line we can approximate the pore surface charge density for zero particle velocity at the center of the pore. The best-fit lines (Fig. 4A) indicate that Particle A will have net zero velocity at a pore charge density of $-6.23\,mC/m^2$, while Particle B becomes stagnant at $-3.64\,mC/m^2$. In other words, within this range (from -6.23 to $-3.64\,mC/m^2$) of pore charge density Particle A has positive velocity, while the velocity of Particle B will be negative. Thus, membrane surface charge density must be set in this range to achieve separation. However, for efficient separation, Particle B should not be permitted to come close to the pore, thus allowing that region to be occupied by Particle A. Figure 4B indicates that to prevent Particle B from reaching within 200 nm to the pore, membrane pore surface charge density should be between -6.58 and $-3.79\,mC/m^2$.

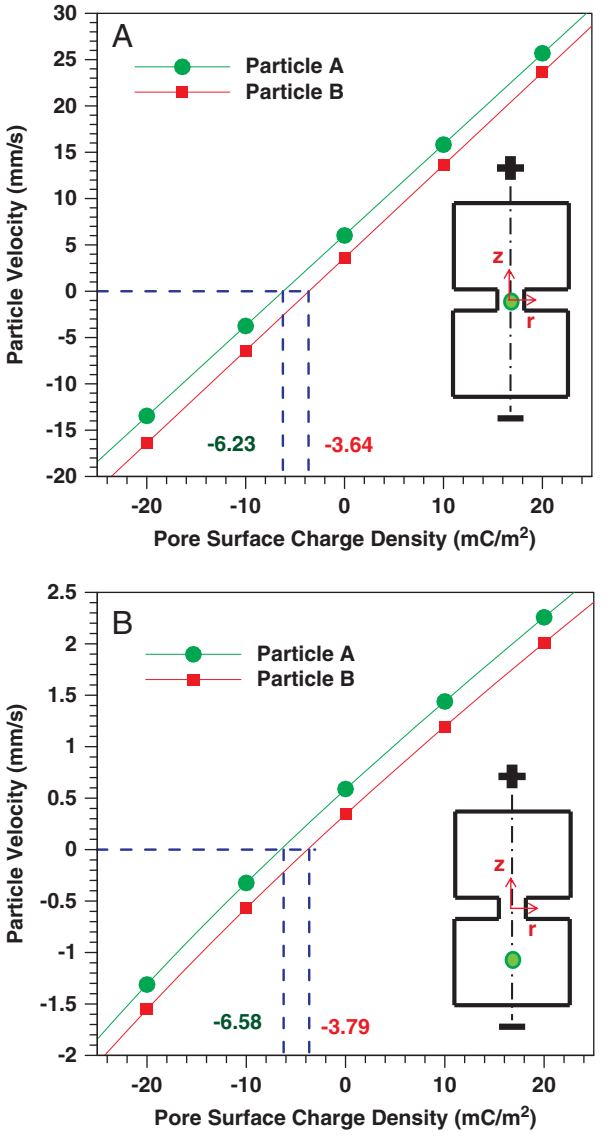

Figure 4. Particle velocity (A) at the center of the pore and (B) 200 nm away from the pore as a function of membrane surface charge density. All other simulation conditions are the same as in Fig. 2.

Based on the outcome of Fig. 4, we selected a membrane surface charge density of $-4.0\,mC/m^2$ to study the motion of Particles A and B. The particle trajectories indicate that only Particle A passes through the pore (Fig. S1(a)), while Particle B moves away from the pore (Fig. S1(b)) when initial position is at $z = -200$ nm. The above single particle-based numerical result suggests that separation of Particle A from B may be possible if the pore surface has a charge density of $\sim -4.0\,mC/m^2$.

5.3 Effect of multiple particles

To validate the above hypothesis, we then simulated the translocation behavior of multiple particles through

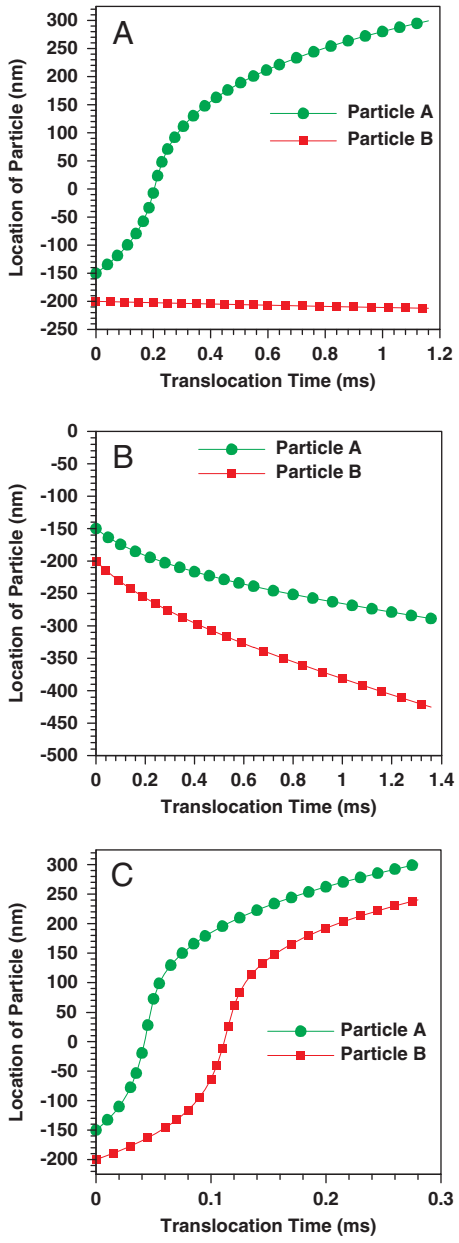

Figure 5. Trajectories of Particle A and Particle B with time for a membrane with a surface charge density of (A) $-4.0\,mC/m^2$, (B) $-8.0\,mC/m^2$, and (C) $4.0\,mC/m^2$. Particles are initially 50 nm apart. All other simulation conditions are the same as in Fig. 2.

the pore for a pore surface charge density of $-4.0\,mC/m^2$. Here, we assumed that Particles A and B are initially located at the centerline of the device, but at two different locations ($z_A = -150$ nm and $z_B = -200$ nm). Figure 5A shows the particle trajectories at different times where Particle A is passing through the pore, while Particle B is moving away from the pore. For Particle A, the electrophoretic force is stronger than the flow field created by the EOF; on the other hand, for Particle B the force field created by electroosmotic flow is bigger than the electrophoretic force.

We have also presented translocation results of Particles A and B for pore surface charge density of $-8.0\,mC/m^2$ (Fig. 5B) and $4.0\,mC/m^2$ (Fig. 5C). In the former case both particles move away from the pore, while in the latter case both particles pass though the pore. For pore surface charge density of $-8.0\,mC/m^2$ (Fig. 5B), electroosmosis dominates the particle translocation and both particles moving away from pore toward cathode. On the other hand, for a positive pore surface charge density (Fig. 5C), both electroosmosis and electrophoresis contribute to the transport of particles toward anode. The particle translocation directions for the abovementioned pore surface cases are in good agreement with the results presented in Fig. 4.

Next, we have investigated the effect of initial separation distance between two particles for a pore surface charge density of $-4.0\,mC/m^2$. Here, the aim was to see how the proximity of one particle affects the other's translocation and separation process. We have varied the initial position of Particle B while keeping Particle A's position constant at $z = -150$ nm. The model suggests that separation of particles is possible regardless of their initial location (Fig. 6). As a matter of fact, the separation distance between two particles does not affect the translocation behavior unless two particles come very close to each other and the EDL of one particle interacts with the other's EDL. From Fig. 6, it can be seen that the position of Particle B remains almost same because of a very small negative (downward) velocity. This suggests that the contributions of electroosmosis and electrophoresis are identical for Particle B when it is away from the pore center. An identical trend is also found in Fig. 7 where the initial position of Particle A is kept constant at -200 nm, while the initial location of Particle B is varied from -150 to -50 nm. In both cases the very minor change in Particle B position is due to the choice of pore charge density ($-4.0\,mC/m^2$) which is very close to the case of zero translocation velocity of Particle B (Fig. 4). On the other hand, if a pore charge density corresponding to the stagnation velocity of Particle A were selected, very little movement of Particle A would have been observed, which is not desirable from the separation point of view. Therefore, to achieve separation, the membrane surface charge density should be selected in such a way that one type of particle should have a strong positive translocation velocity.

Figure 7 also reveals that an axisymmetric model will not be able to predict the separation process if a Particle B is located above a Particle A. In this case, Particle A will continue to move toward the anode due the electrophoretic motion but it will not be able to bypass the very slow moving particle B which is blocking Particle A's translocation route. However, the model suggests that Particle B will not translocate through the nanopore if the pore surface charge density is $\sim -4.0\,mC/m^2$. In reality, Particle B has very low probability of coming close to the pore because of the negligible translocation velocity, and only Particle A would dominate the region close to t he pore.

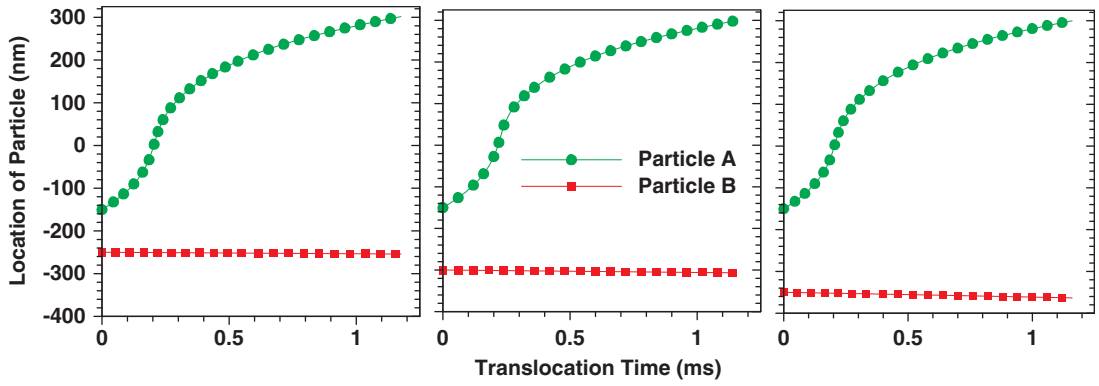

Figure 6. Trajectories of Particle A and Particle B with initial separation distance (left) 100 nm, (middle) 150 nm, and (right) 200 nm for a surface charge density $\sigma_m = -4.0\ mC/m^2$. All other simulation conditions are the same as in Fig. 2.

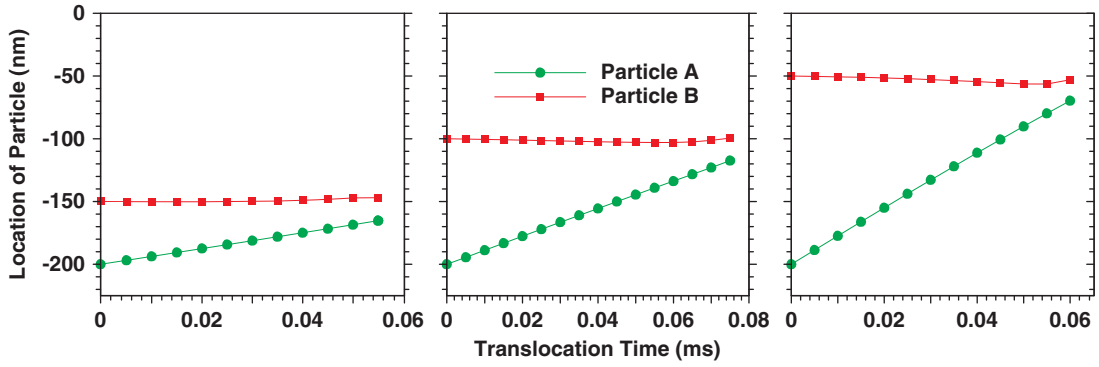

Figure 7. Trajectories of Particle A and Particle B with an initial separation distance (left) 50 nm, (middle) 100 nm, and (right) 150 nm for a pore surface charge density $\sigma_m = -4.0\ mC/m^2$. All other simulation conditions are same as in Fig. 2.

6 Concluding remarks

A mathematical model for electrokinetic transport of nanoparticles through a nanopore was developed to study particle translocation and then find optimum design for LDL apheresis. Considering the length scale disparity, we implemented a multi-length scale model for particle translocation. Coarse grids were used to compute the flow and electric field in the device-level simulation, and a relatively smaller domain was selected close to the pore where finer grids were employed to calculate the electrokinetic forces using boundary conditions obtained from the regular domain simulation. The numerical results were compared with experimental data and a good agreement was obtained between them.

In order to design a nanofluidic platform for LDL apheresis, the effect of the pore thickness, radius, and surface charge density were studied. Numerical simulations reveal that the pore thickness and radius affect the particle velocity at the center of pore, but they cannot be used as a control parameter for particle separation. It has been shown that for a particular range of pore surface charge densities, the electroosmotic flow can be tailored so that the membrane is permeable to only one type of particle. Our numerical results show that pore surface charge density $\sim -4.0\ mC/m^2$ is suitable for separation of LDL like particle from HDL. We also found that the initial location of particles does not change the separation mechanism.

The authors have declared no conflict of interest.

7 References

[1] Humes, H. D., Fissell, W. H., Tiranathanagul, K., *Kidney Int.* 2006, *69*, 1115–1119.

[2] Thompson, G. R., *Atherosclerosis* 2003, *167*, 1–13.

[3] Yang, F., Yang, X. M., Jiang, H., Bulkhaults, P., Wood, P., Hrushesky, W., Wang, G. R., *Biomicrofluidics* 2010, *4*, 013204.

[4] Fu, J. P., Mao, P., Han, J., *Trends Biotechnol.* 2008, *26*, 311–320.

[5] Tegenfeldt, J. O., Prinz, C., Cao, H., Huang, R. L., Austin, R. H., Chou, S. Y., Cox, E. C., Sturm, J. C., *Anal. Bioanal. Chem.* 2004, *378*, 1678–1692.

[6] Craighead, H., *Nature* 2006, *442*, 387–393.

[7] Kim, M. J., Wanunu, M., Bell, D. C., Meller, A., *Adv. Mater.* 2006, *18*, 3149–3153.

[8] Storm, A. J., Chen, J. H., Ling, X. S., Zandbergen, H. W., Dekker, C., *Nat. Mater.* 2003, *2*, 537–540.

[9] Park, S. R., Peng, H. B., Ling, X. S. S., *Small* 2007, *3*, 116–119.

[10] Duan, C. H., Majumdar, A., *Nat. Nanotechnol.* 2010, *5*, 848–852.

[11] Savariar, E. N., Krishnamoorthy, K., Thayumanavan, S., *Nat. Nanotechnol.* 2008, *3*, 112–117.

[12] Karnik, R., Castelino, K., Majumdar, A., *Appl. Phys. Lett.* 2006, *88*, 123114.

[13] Kuo, T. C., Sloan, L. A., Sweedler, J. V., Bohn, P. W., *Langmuir* 2001, *17*, 6298–6303.

[14] Striemer, C. C., Gaborski, T. R., McGrath, J. L., Fauchet, P. M., *Nature* 2007, *445*, 749–753.

[15] Kasianowicz, J. J., Robertson, J. W. F., Chan, E. R., Reiner, J. E., Stanford, V. M., *Annu. Rev. Anal. Chem.* 2008, *1*, 737–766.

[16] Firnkes, M., Pedone, D., Knezevic, J., Doblinger, M., Rant, U., *Nano Lett.* 2010, *10*, 2162–2167.

[17] Prabhu, A. S., Jubery, T. Z. N., Freedman, K. J., Mulero, R., Dutta, P., Kim, M. J., *J. Phys. – Condens. Matter* 2010, *22*, 454107.

[18] Heng, J. B., Ho, C., Kim, T., Timp, R., Aksimentiev, A., Grinkova, Y. V., Sligar, S., Schulten, K., Timp, G., *Biophys. J.* 2004, *87*, 2905–2911.

[19] Karniadakis, G., Beskok, A., Aluru, N., *Microflows and Nanoflows*, Springer, Berlin 2005.

[20] Liu, H., Qian, S. Z., Bau, H. H., *Biophys. J.* 2007, *92*, 1164–1177.

[21] Chein, R. Y., Dutta, P., *Colloids Surfaces: A Physicochem. Eng. Asp.* 2009, *341*, 1–12.

[22] Dutta, P., Beskok, A., Warburton, T. C., *Numer. Heat Tranf. A – Appl.* 2002, *41*, 131–148.

[23] Kirby, B. J., *Micro- and Nanoscale Fluid Mechanics: Transport in Microfluidic Devices*, Cambridge University Press, Cambridge 2010.

[24] Wu, M. B., Kuznetsov, A. V., Jasper, W. J., *Phys. Fluids* 2010, *22*, 043301.

[25] Hsu, J. P., Hung, S. H., Kao, C. Y., Tseng, S., *Chem. Eng. Sci.* 2003, *58*, 5339–5347.

